JACS
JOURNAL OF THE AMERICAN CHEMICAL SOCIETY

pubs.acs.org/JACS

Article

All-Carbon-Linked Continuous Three-Dimensional Porous Aromatic Framework Films with Nanometer-Precise Controllable Thickness

Martin Ratsch, Chen Ye, Yizhou Yang, Airui Zhang, Austin M. Evans, and Karl Börjesson*

Cite This: J. Am. Chem. Soc. 2020, 142, 6548−6553

Read Online

ACCESS | Metrics & More | Article Recommendations | Supporting Information

ABSTRACT: Inherently porous materials that are chemically and structurally robust are challenging to construct. Conventionally, dynamic chemistry is thought to be needed for the formation of uniform porous organic frameworks, but dynamic bonds can limit the stability of these materials. For this reason, all-carbon-linked frameworks are expected to exhibit higher stability performance than more traditional porous frameworks. However, the limited reversibility of carbon−carbon bond-forming reactions has restricted the exploration of these materials. In particular, the challenges associated with producing uniform thin films of all-carbon-linked frameworks has inhibited the study of these materials in applications where well-defined films are required. Here, we synthesize continuous and homogeneous films of two different all-carbon-linked three-dimensional porous aromatic frameworks with nanometer-precision thickness (PAF-1 and BCMP-2). This was accomplished by kinetically promoting surface reactivity while suppressing homogeneous nucleation. Through connection of the PAF film to a gold substrate via a self-assembled monolayer and use of flow conditions to continually introduce monomers, smooth and continuous PAF films can be grown with controlled thickness. This strategy allows traditional transition metal mediated carbon−carbon cross-coupling reactions to form porous, organic thin films. We expect that the chemical principles uncovered in this study will enable the synthesis of a variety of chemically and structurally diverse carbon−carbon-linked frameworks as high-quality films, which are inaccessible by conventional methods.

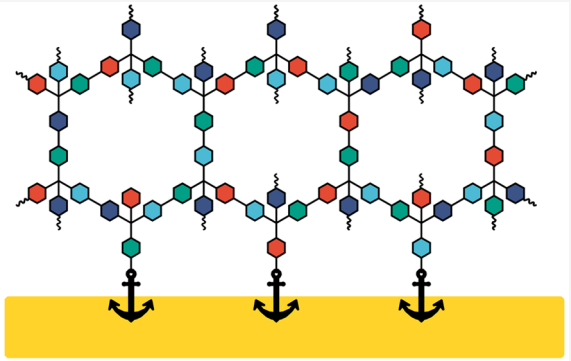

INTRODUCTION

Covalent organic frameworks (COFs) were first synthesized by Yaghi and co-workers in 2005 and represent a class of porous, structurally regular materials that contain only light elements (i.e., B, C, N, H, and O).[1] Organic framework materials have a unique suite of properties such as ultrahigh thermal stability (up to 500 °C),[2,3] low densities (0.13 g cm^{-3}),[4] and high internal surface area (7000 m^2 g^{-1}).[5] This confluence of properties make this class of materials highly suitable for various applications such as chemical separations,[6−8] catalysis,[9−11] gas storage,[12−14] water purification,[15] drug delivery,[16−18] electrode materials,[19,20] and sensing.[21] Porous aromatic frameworks (PAFs) are siblings of COFs, which are synthesized by irreversible cross-coupling reactions. Because these materials are unable to anneal defects, due to the irreversible nature of their chemical linkages, PAFs are frequently thought to have a disordered nanoscale structure. In three-dimensional (3D) organic frameworks, nonplanar building blocks are covalently cross-linked in all dimensions.[2,4,22−29] This topology leads to channels in all dimensions, with pore spaces of defined shape and size that can be chemically engineered according to a desired function.[11,30,31] We find that 3D frameworks are underrepresented in the literature compared to two-dimensional (2D) variants. In particular, films of 3D frameworks are especially challenging to synthesize and represent a frontier in synthetic framework chemistry. We speculate that this limited exploration is partially due to the higher difficulty in synthesizing homogeneous films of 3D organic frameworks compared to 2D variants.[32] This difficulty is accentuated when considering the synthesis of carbon−carbon-linked 3D frameworks; whose defects cannot be annealed through dynamic chemistry.

Although 3D COFs and PAFs have been synthesized as microcrystalline powders, many promising applications (e.g., membranes or electronics) for these materials will require films.[33] This understanding has inspired immense interest in synthesizing COFs and PAFs as uniform films, which can be more readily interfaced with these applications. Recently, films of 2D frameworks have been made on templated surfaces using batch solvothermal conditions.[34,35] Other strategies for the synthesis of uniform 2D films include exfoliation and

Received: October 10, 2019
Published: March 18, 2020

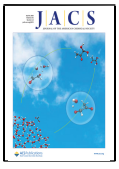

https://dx.doi.org/10.1021/jacs.9b10884
J. Am. Chem. Soc. 2020, 142, 6548−6553

reassembly,[36] interfacial crystallization of thin 2D films at liquid−liquid[37] or air−liquid interfaces,[38] and blade casting of precursors.[6] Expanding on these batch reaction approaches, Bisbey and co-workers used a continuous flow setup in combination with a quartz crystal microbalance to measure the deposited mass of a 2D COF on a Ti surface in real time, giving control of the film thickness.[39] However, topological differences between 2D and 3D frameworks mean that methods used to construct 2D-based films cannot be readily adapted for 3D framework film synthesis. Films of 3D COFs have been made using dynamic imine or boronate ester bonds.[40] However, to date, the only example of an all carbon-linked 3D framework was described by Becker and co-workers in 2015, where they used a templated surface and batch conditions to form a 3D PAF-1 film with micrometer-scale roughness.[41] Although this report shows that carbon−carbon-bonded 3D frameworks can be obtained as films, they showed unwieldy surface roughness, powder contamination, and unpredictable thickness. However, this preliminary report led us to speculate that the synthesis of smooth 3D framework films with precise thickness based on carbon−carbon bonds is now within reach, a crucial step toward maximizing the utility of this class of promising materials.

Here, we show for the first time that it is possible to construct all-carbon-linked 3D PAFs as smooth and continuous films with controllable thicknesses. This new synthesis method works by introducing monomers at low steady-state concentrations in flow to a pretemplated substrate. This approach favors film growth over bulk powder synthesis, which can contaminate the desired films. A quartz crystal microbalance (QCM) was used to monitor the growth of the film in real time and scanning electron microscopy (SEM) cross-section imaging was used to correlate the QCM signal to film thickness, allowing for nanometer thickness control. Continuous flow conditions constantly remove in-bulk-formed oligomers, resulting in an improved smoothness of the obtained film by limiting the precipitation of bulk framework materials. Films were further characterized via depth-dependent X-ray photoelectron spectroscopy (XPS) and energy dispersive X-ray spectroscopy-scanning electron microscopy (EDX-SEM), which show that the desired C−C polymerization chemistry had taken place. Furthermore, surface roughness was probed by atomic force microscopy (AFM), which demonstrated that the films were smooth, continuous, and free from powder contamination. This work provides a strategy to overcome the former restrictions of 3D film synthesis that we suspect will enable the construction of a broad range of porous materials in a useful configuration for a host of applications.

RESULTS AND DISCUSSION

To construct a film of framework material, it is crucial to spatially control polymerization. For example, frameworks synthesized by homocoupling of a single monomer species can occur between monomers and oligomers in solution or between monomers and the film surface. C−C bonds are robust, providing rigidity and chemical stability to the obtained structure. However, C−C cross-coupling prevents dynamic rearrangement, which prevents defects from being annealed. Once the bonds are formed, they do not break and a kinetically favored rather than the thermodynamically favored product may be trapped. Therefore, we hypothesize that initial formation of a structurally regular material will be necessary for the synthesis of smooth, homogeneous films. Additionally, if precise thicknesses, low roughness films are to be obtained, the film must be synthesized epitaxially. However, the same reaction that leads to productive surface growth may also take place in solution, resulting in larger aggregates that can contaminate the film. Stated another way, the challenge is to restrict homogeneous nucleation of framework powders while promoting uniform, layer-by-layer heterogeneous growth of framework films.[42,43]

The reaction rate between two species, whether monomers or oligomers, in solution is expected to follow second-order kinetics with respect to the concentration of the monomer. In contrast, when the monomer couples to the surface, the concentration of one of the reactants (the surface) is fixed and so pseudo-first-order kinetics would be expected. Thus, the relevant rate equations for the monomer−monomer and the monomer−surface reactions are as follows:

$$r_{\text{bulk}} = k_{\text{bulk}}[\text{monomer}]^2 \quad (1)$$

$$r_{\text{surface}} = k'_{\text{surface}}[\text{monomer}] \quad (2)$$

where r is the reaction rate and k is the relevant reduced rate constant (including the concentration of non-monomeric coupling reagents, catalysts, etc.). This difference in reaction kinetics indicates that, at high concentration, monomers will predominantly react to form oligomers, which at some critical size will precipitate from solution. When the concentration is reduced, the bulk reaction will be reduced in comparison to surface growth. Therefore, below a certain concentration threshold, the reaction on the surface will dominate, which we hypothesize would be ideal for the synthesis of uniform C−C-linked framework films. To show that it is possible to synthesize a continuous framework film, we chose the well-known PAF system PAF-1[5,44] (also published as PPN-6).[45] In PAF-1, tetrakis(4-bromophenyl)methane (TBPM; Figure 1) is used as a building block, which forms a 3D network via Yamamoto coupling.[46] PAF-1 has an exceptionally high surface area and excellent hydrothermal stability because of the

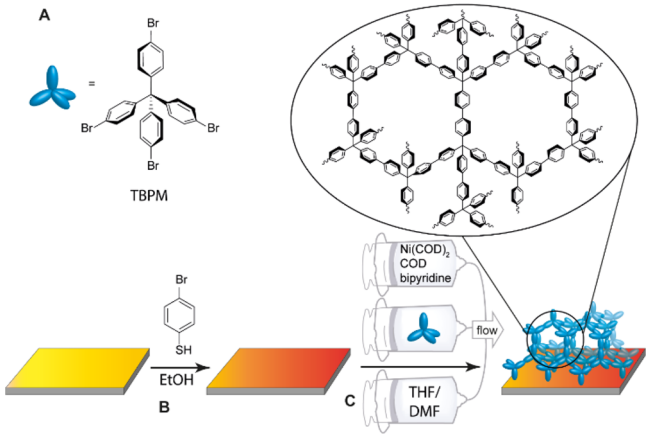

Figure 1. Schematic overview of the reaction on the surface leading to a continuous film. (A) Building block, tetrakis(4-bromophenyl)-methane (TBPM). (B) Self-assembled monolayer (SAM) formation on the gold QCM chips. (C) Continuous flow setup with three autonomous programmable syringe pumps pushing the fluids through the QCM chamber where the reaction on the surface takes place, forming the COF film.

https://dx.doi.org/10.1021/jacs.9b10884
J. Am. Chem. Soc. 2020, 142, 6548−6553

chemical stability of the C−C bond and its powders have found use in gas storage applications.[5]

When making a film via a bottom-up approach, adhesion between the substrate and the first layer of the framework film is necessary. Because thiols are known to diffuse laterally on Au surfaces, giving the possibility for structures attached by such bonds to self-organize, we selected a thiol functionalization strategy to create a well-adhered first layer of the film. To achieve this, we exposed a gold-coated QCM wafer to 4-bromothiophenol, which forms a self-assembled monolayer on the gold surface (Figure 1).[41] This molecule is bromine-functionalized at the para-position, allowing for Yamamoto coupling reaction with the PAF-1 monomer (TBPM). We expect that a fully thiol-functionalized SAM will react with the appropriate number of TBPMs to yield a monolayer that will serve as a template for PAF formation. Previously, researchers have used a thiol-templated surface to connect PAF-1 to a surface.[41] We have extended this strategy to yield continuous 3D PAF films by the following: (1) limiting the steady-state concentration of the monomer to about 1% of the concentration previously demonstrated to synthesize PAF-1,[41] and (2) using continuous flow conditions that provide clean reagents throughout the reaction and limit powder aggregation. To accommodate these adaptations, we built a continuous flow cell setup based on three programmable syringe pumps, a mixing unit, and a quartz crystal microbalance (QCM) flow cell (Figure 1). The monomer and coupling reagents were kept in separate syringes and mixed just before entering the QCM flow cell. Figure 2 displays microscope

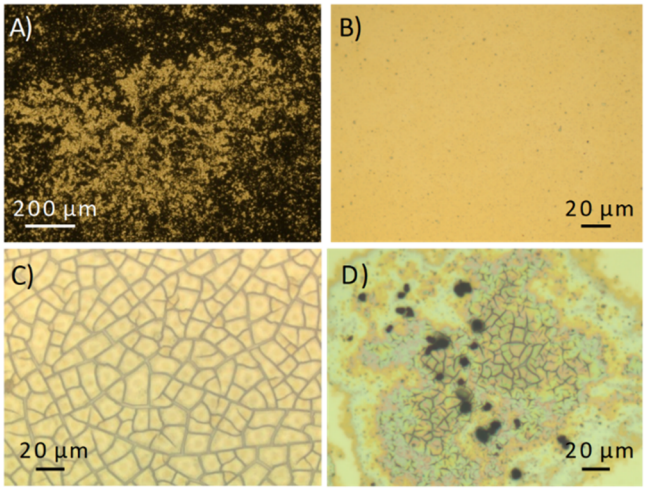

Figure 2. Optical images of PAF-1 films. (A) Batch mode: An immersed templated gold sensor in a solution of monomers and coupling reagents, leading to a macroscopic nonuniform surface. (B) Continuous flow: Mixing of monomers and coupling reagents just before the flow reactor leads to a continuous and smooth film. (C) Continuous flow: Numerous cracks are evident when using a nonbrominated SAM under the same reaction conditions. (D) Continuous flow: Cracks and powder contamination are also present when using a 10-fold higher concentration than those used in B.

images of films made using bulk or flow conditions. In bulk conditions, the film is very rough (Figure 2A), which is consistent with previously reported approaches.[41] We suspect that, in this case, oligomers have mostly first formed in solution and later bind to the surface, providing macroscopic nonuniform structures. On the other hand, flow conditions produce a film that is smooth on a macroscopic level, as evident from the absence of scattering in the uniform microscope image (Figure 2B). If thiophenol instead of 4-bromothiophenol is used in the SAM layer, the ability to form covalent bonds between the SAM and the porous film is removed (Figure 2C). This results in cracks between relatively flat regions. The lack of connection between the surface and the framework most likely results in PAF grains first precipitating on the surface, and these grains then grow. Cracks and an uneven distribution could also be observed when using flow conditions with a 10 times higher concentration of all reagents (Figure 2D) when compared to the conditions used in Figure 2B. Furthermore, the surface roughness (as measured with AFM) increased when increasing the concentrations above a certain point (Figure S1). High-concentration conditions also resulted in the formation of visible aggregates in the tubing after the mixing unit. These experiments demonstrate that surface connectivity, low concentration, and flow conditions are needed to form a uniform framework film. In the next section, we examine the buildup of the film in real time, enabling the construction of films with nanometer precision thickness.

To monitor the buildup of the framework film in real time, we used a QCM. QCM measures the mass change as a shift of the quartz resonance frequency over time. The frequency shift correlates directly to the thickness of the film, and the slope of the frequency shift relates to the reaction rate on the film surface. Figure 3A displays the frequency shift as a function of

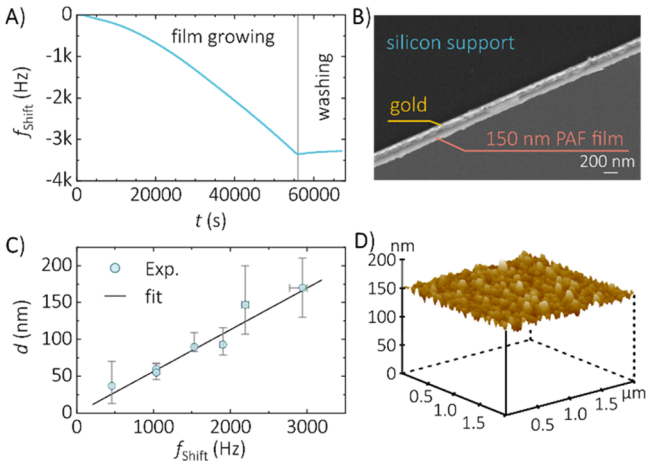

Figure 3. Monitoring the film growth. (A) Typical frequency change during the reaction. (B) SEM picture with 69000× magnification of the film cross section, showing the existence of a smooth film. (C) Plot showing a linear correlation between the frequency change and the film thickness. (D) AFM image of a 150 nm thick film, having a mean square roughness of 4 nm.

reaction time. A nearly linear dependence between the frequency shift versus time is evident, indicating that the rate of reaction on the surface is constant when the monomer concentration is held constant, as indicated by eq 2. However, when the flow speed is reduced under the same concentration, a lower slope in the frequency shift over time was observed (Figure S2). The boundary layer is the area of the fluid close to the solid surface (in our case the surface of the film). The velocity of the fluid in the boundary layer decreases toward zero when approaching the surface. The only possibility for building blocks to reach the surface is therefore via diffusion through this layer. The thickness of the boundary layer is flow-

https://dx.doi.org/10.1021/jacs.9b10884
J. Am. Chem. Soc. 2020, 142, 6548−6553

speed-dependent. When the flow speed is reduced, the thickness of the boundary layer increases, which causes a reduction in the growth rate.[47] This observation suggests that the reaction rate on the surface is limited by mass transport close to the surface, which is affected by the flow speed. Furthermore, SEM showed a completely flat film within the spatial resolution of the instrument (Figure 3B, Figures S3 and S4), and AFM showed a mean roughness of less than 4 nm over an area of 4 μm^2 (Figure 3D). The formed films can therefore be regarded as homogeneous on the macroscopic scale and smooth on the nanoscale.

To correlate the frequency shift to film thickness, we broke QCM chips and performed cross-section imaging via SEM (Figure 3B). Figure 3C displays a linear relation between film thickness (as measured with SEM) and frequency shift (measured with QCM), indicating that the mass density profile of the film is homogeneous. This finding allowed us to calculate the frequency to thickness relationship to 0.057 nm Hz^{-1}. We considered the possibility that encaged solvent molecules might influence the frequency shift and thus the measured mass. To see whether solvent contributes to the frequency shift, we compared the change in frequency shift of a film and a clean gold surface when changing the solvent from tetrahydrofuran (THF) to deuterated THF (Figure S5). We observed a difference between the two substrates, indicating that caged solvent molecules do influence the measured weight. Thus, the observed frequency shift originates not only from the film but also from caged solvent molecules. Furthermore, the constant relating frequency shift to film thickness is therefore dependent on the solvent used. Interested in evaluating the porous structure of our PAF-1 films, we evaluated the electron density with X-ray reflectivity measurements. We find that the electron density is approximately ~0.6 $e^- Å^{-3}$ (Figure S7). Although this is nearly double an idealized structure, we expect that structural defects, framework intercalation, residual solvent, and catalyst would all lead to more dense structures than that of the ideal PAF-1. Importantly, similarly dense PAF-1 materials have also been found to have exceptional surface areas.[48] This finding is consistent with the understanding that solvent molecules are intercalated into the framework (Figure S5), giving rise to solvent-dependent shifts of the observed QCM frequency. Thus, by controlling the introduction of monomers to a pretemplated surface, it is possible to create smooth, porous 3D framework films with controllable thicknesses.

To examine the chemical composition of the formed film on top of a gold substrate, we measured the XPS signal as a function of etching time. Figure 4A,B shows the carbon and gold content of the film and substrate at varying etching times. At a short distance into the film, only a carbon signal was observed, consistent with the signal from PAF-1. In contrast, deeper in the sample, the carbon signal vanished and the signal from the gold substrate concurrently appeared. This XPS analysis is consistent with our understanding of a fully carbon–hydrogen framework adhered to the gold substrate. The element composition was also explored on a film cross section (Figure 4C–E) using EDX-SEM. By targeting the film on the sensor surface (bright gray in B), we found the main elements to be gold, chromium, and carbon. The gold signal arises from the roughly 100 nm thick gold coating on the sensor and chromium is used as an adhesive layer between gold and the silicon crystal. The carbon signal originates from the deposited film. Measuring further away from the PAF-1 film, deeper into

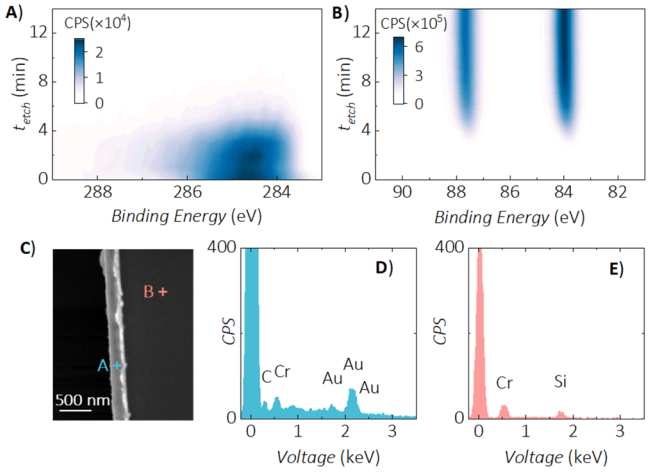

Figure 4. Confirming the elemental composition. (A, B) Depth XPS spectrum, showing the existence of gold (B) right underneath the carbon (A) containing film. (C–E) EDX-SEM measurements on the cross section of a film. The elements shown in area A (blue) match the existence of a PAF-1 based film (carbon) and the gold surface on chromium (very thin adhesive layer between silicon and gold). Area B (red) shows the existence of silicon (quartz crystal) and Cr.

the sensor, only silicon and chromium gave prominent signals. The measured element composition matched the information given by the manufacturer (Biolin Scientific), further confirming the expected element composition of the PAF film (see Figures S3 and S4 for additional SEM images and EDX spectra).

In principle, the understanding of controlled polymerization at a functionalized surface should be general to an array of carbon–carbon bond-forming reactions. To expand on the generality of the described method, we also made films by subjecting TBPM and 1,4-diethynylbenzene to Sonogashira coupling conditions. PAF powders synthesized in previous reports using these building blocks are reported as BCMP-2.[49] One conceptual difference between PAF-1 and BCMP-2 is that PAF-1 is based on a homocoupling of a single reactant whereas BCMP-2 is based on the heterocoupling of two distinct reactants. Nonetheless, our approach for the synthesis of uniform homocoupled films easily accommodated the synthesis of heterocoupled 3D PAFs (Figures S8 and S9). A nearly linear mass increase with time is evident by following the Sonogashira reaction in flow using QCM. Furthermore, by decreasing the concentration of the building blocks, we observed a reduced surface roughness until a plateau value is reached. Generally, all organic framework materials are made by either homocouplings or heterocouplings and smooth films of both can be made by employing the methodology developed here.

CONCLUSION

We have successfully constructed continuous and smooth films of two different 3D porous aromatic frameworks with nanometer-precise controllable thickness. QCM was used to provide real-time monitoring of the film growth and cross-section SEM was used to correlate the QCM signal to film thickness. This was realized by continually introducing a sufficiently low steady-state concentration of monomers to a pretemplated surface. The approach is based on fundamental chemical principles, and we therefore believe it will enable the synthesis of a variety of 3D carbon-linked framework materials

https://dx.doi.org/10.1021/jacs.9b10884
J. Am. Chem. Soc. 2020, 142, 6548–6553

as uniform films. Furthermore, we envision that the modular flow approach described here can be used to make heterostructured framework films. We suspect that by flowing different monomers in series, one can assemble diverse framework materials sequentially within a continuous film. This approach of making 3D framework films opens up this class of material to applications where robustly adhered films of all-carbon-linked porous material is required.

■ ASSOCIATED CONTENT

Supporting Information

The Supporting Information is available free of charge at https://pubs.acs.org/doi/10.1021/jacs.9b10884.

Details including experimental details, synthetic procedure, and Figures S1−S9 (PDF)

■ AUTHOR INFORMATION

Corresponding Author

Karl Börjesson − *Department of Chemistry and Molecular Biology, University of Gothenburg, 412 96 Göteborg, Sweden;* orcid.org/0000-0001-8533-201X; Email: karl.borjesson@gu.se

Authors

Martin Ratsch − *Department of Chemistry and Molecular Biology, University of Gothenburg, 412 96 Göteborg, Sweden*

Chen Ye − *Department of Chemistry and Molecular Biology, University of Gothenburg, 412 96 Göteborg, Sweden*

Yizhou Yang − *Department of Chemistry and Molecular Biology, University of Gothenburg, 412 96 Göteborg, Sweden;* orcid.org/0000-0002-0331-6815

Airui Zhang − *Division of Energy and Environmental Measurement, National Institute of Metrology, China NIM, Beijing 100013, P.R. China*

Austin M. Evans − *Department of Chemistry, Northwestern University, Evanston, Illinois 60208, United States;* orcid.org/0000-0002-3597-2454

Complete contact information is available at: https://pubs.acs.org/10.1021/jacs.9b10884

Notes

The authors declare no competing financial interest.

■ ACKNOWLEDGMENTS

We gratefully acknowledge the financial support from the Swedish Research Council (2016-03354). Martin Andersson is acknowledged for providing access to QCM apparatus and Anders Mårtensson is acknowledged for help with AFM measurements. A.M.E. is supported by the National Science Foundation Graduate Research Fellowship under grant no. (DGE-1324585). This work made use of the Jerome B. Cohen X-ray Diffraction Facility supported by the MRSEC program of the National Science Foundation (DMR-1720139) at the Materials Research Center of Northwestern University and the Soft and Hybrid Nanotechnology Experimental (SHyNE) Resource (NSF ECCS-1542205).

■ REFERENCES

(1) Cote, A. P.; Benin, A. I.; Ockwig, N. W.; O'Keeffe, M.; Matzger, A. J.; Yaghi, O. M. Porous, crystalline, covalent organic frameworks. *Science* **2005**, *310* (5751), 1166−1170.

(2) El-Kaderi, H. M.; Hunt, J. R.; Mendoza-Cortes, J. L.; Cote, A. P.; Taylor, R. E.; O'Keeffe, M.; Yaghi, O. M. Designed synthesis of 3D covalent organic frameworks. *Science* **2007**, *316* (5822), 268−272.

(3) Evans, A. M.; Ryder, M. R.; Flanders, N. C.; Vitaku, E.; Chen, L. X.; Dichtel, W. R. Buckling of Two-Dimensional Covalent Organic Frameworks under Thermal Stress. *Ind. Eng. Chem. Res.* **2019**, *58* (23), 9883−9887.

(4) Baldwin, L. A.; Crowe, J. W.; Pyles, D. A.; McGrier, P. L. Metalation of a Mesoporous Three-Dimensional Covalent Organic Framework. *J. Am. Chem. Soc.* **2016**, *138* (46), 15134−15137.

(5) Ben, T.; Ren, H.; Ma, S. Q.; Cao, D. P.; Lan, J. H.; Jing, X. F.; Wang, W. C.; Xu, J.; Deng, F.; Simmons, J. M.; Qiu, S. L.; Zhu, G. S. Targeted Synthesis of a Porous Aromatic Framework with High Stability and Exceptionally High Surface Area. *Angew. Chem., Int. Ed.* **2009**, *48* (50), 9457−9460.

(6) Kandambeth, S.; Biswal, B. P.; Chaudhari, H. D.; Rout, K. C.; Kunjattu H, S.; Mitra, S.; Karak, S.; Das, A.; Mukherjee, R.; Kharul, U. K.; Banerjee, R. Selective Molecular Sieving in Self-Standing Porous Covalent-Organic-Framework Membranes. *Adv. Mater.* **2017**, *29* (2), 1603945.

(7) Zhao, H.; Jin, Z.; Su, H.; Zhang, J.; Yao, X.; Zhao, H.; Zhu, G. Target synthesis of a novel porous aromatic framework and its highly selective separation of CO_2/CH_4. *Chem. Commun.* **2013**, *49* (27), 2780−2782.

(8) Lu, W. G.; Yuan, D. Q.; Zhao, D.; Schilling, C. I.; Plietzsch, O.; Muller, T.; Brase, S.; Guenther, J.; Blumel, J.; Krishna, R.; Li, Z.; Zhou, H. C. Porous Polymer Networks: Synthesis, Porosity, and Applications in Gas Storage/Separation. *Chem. Mater.* **2010**, *22* (21), 5964−5972.

(9) Pachfule, P.; Acharjya, A.; Roeser, J.; Langenhahn, T.; Schwarze, M.; Schomäcker, R.; Thomas, A.; Schmidt, J. Diacetylene Functionalized Covalent Organic Framework (COF) for Photocatalytic Hydrogen Generation. *J. Am. Chem. Soc.* **2018**, *140* (4), 1423−1427.

(10) Bhadra, M.; Kandambeth, S.; Sahoo, M. K.; Addicoat, M.; Balaraman, E.; Banerjee, R. Triazine Functionalized Porous Covalent Organic Framework for Photo-organocatalytic E−Z Isomerization of Olefins. *J. Am. Chem. Soc.* **2019**, *141* (15), 6152−6156.

(11) Ding, S.-Y.; Wang, W. Covalent organic frameworks (COFs): from design to applications. *Chem. Soc. Rev.* **2013**, *42* (2), 548−568.

(12) Konstas, K.; Taylor, J. W.; Thornton, A. W.; Doherty, C. M.; Lim, W. X.; Bastow, T. J.; Kennedy, D. F.; Wood, C. D.; Cox, B. J.; Hill, J. M.; Hill, A. J.; Hill, M. R. Lithiated Porous Aromatic Frameworks with Exceptional Gas Storage Capacity. *Angew. Chem., Int. Ed.* **2012**, *51* (27), 6639−6642.

(13) Huang, N.; Chen, X.; Krishna, R.; Jiang, D. Two-Dimensional Covalent Organic Frameworks for Carbon Dioxide Capture through Channel-Wall Functionalization. *Angew. Chem., Int. Ed.* **2015**, *54* (10), 2986−2990.

(14) Lee, G.-Y.; Lee, J.; Vo, H. T.; Kim, S.; Lee, H.; Park, T. Amine-Functionalized Covalent Organic Framework for Efficient SO2 Capture with High Reversibility. *Sci. Rep.* **2017**, *7* (1), 557.

(15) Fernandes, S. P. S.; Romero, V.; Espiña, B.; Salonen, L. M. Tailoring Covalent Organic Frameworks To Capture Water Contaminants. *Chem. - Eur. J.* **2019**, *25* (26), 6461−6473.

(16) Bai, L.; Phua, S. Z. F.; Lim, W. Q.; Jana, A.; Luo, Z.; Tham, H. P.; Zhao, L.; Gao, Q.; Zhao, Y. Nanoscale covalent organic frameworks as smart carriers for drug delivery. *Chem. Commun.* **2016**, *52* (22), 4128−4131.

(17) Zhang, G.; Li, X.; Liao, Q.; Liu, Y.; Xi, K.; Huang, W.; Jia, X. Water-dispersible PEG-curcumin/amine-functionalized covalent organic framework nanocomposites as smart carriers for in vivo drug delivery. *Nat. Commun.* **2018**, *9* (1), 2785.

(18) Mitra, S.; Sasmal, H. S.; Kundu, T.; Kandambeth, S.; Illath, K.; Díaz Díaz, D.; Banerjee, R. Targeted Drug Delivery in Covalent Organic Nanosheets (CONs) via Sequential Postsynthetic Modification. *J. Am. Chem. Soc.* **2017**, *139* (12), 4513−4520.

(19) Wu, Y.; Yan, D.; Zhang, Z.; Matsushita, M. M.; Awaga, K. Electron Highways into Nanochannels of Covalent Organic Frame-

works for High Electrical Conductivity and Energy Storage. *ACS Appl. Mater. Interfaces* **2019**, *11* (8), 7661−7665.
(20) Wang, M.; Guo, H.; Xue, R.; Li, Q.; Liu, H.; Wu, N.; Yao, W.; Yang, W. Covalent Organic Frameworks: A New Class of Porous Organic Frameworks for Supercapacitor Electrodes. *ChemElectroChem* **2019**, *6*, 2984.
(21) Wu, X.; Han, X.; Xu, Q.; Liu, Y.; Yuan, C.; Yang, S.; Liu, Y.; Jiang, J.; Cui, Y. Chiral BINOL-Based Covalent Organic Frameworks for Enantioselective Sensing. *J. Am. Chem. Soc.* **2019**, *141* (17), 7081−7089.
(22) Chen, Y.; Shi, Z.-L.; Wei, L.; Zhou, B.; Tan, J.; Zhou, H.-L.; Zhang, Y.-B. Guest-Dependent Dynamics in a 3D Covalent Organic Framework. *J. Am. Chem. Soc.* **2019**, *141* (7), 3298−3303.
(23) Yang, Y.; Goh, K.; Weerachanchai, P.; Bae, T.-H. 3D covalent organic framework for morphologically induced high-performance membranes with strong resistance toward physical aging. *J. Membr. Sci.* **2019**, *574*, 235−242.
(24) Liu, Y.; Diercks, C. S.; Ma, Y.; Lyu, H.; Zhu, C.; Alshmimri, S. A.; Alshihri, S.; Yaghi, O. M. 3D Covalent Organic Frameworks of Interlocking 1D Square Ribbons. *J. Am. Chem. Soc.* **2019**, *141* (1), 677−683.
(25) Han, X.; Huang, J.; Yuan, C.; Liu, Y.; Cui, Y. Chiral 3D Covalent Organic Frameworks for High Performance Liquid Chromatographic Enantioseparation. *J. Am. Chem. Soc.* **2018**, *140* (3), 892−895.
(26) Brucks, S. D.; Bunck, D. N.; Dichtel, W. R. Functionalization of 3D covalent organic frameworks using monofunctional boronic acids. *Polymer* **2014**, *55* (1), 330−334.
(27) Bunck, D. N.; Dichtel, W. R. Postsynthetic functionalization of 3D covalent organic frameworks. *Chem. Commun.* **2013**, *49* (24), 2457−2459.
(28) Yahiaoui, O.; Fitch, A. N.; Hoffmann, F.; Fröba, M.; Thomas, A.; Roeser, J. 3D Anionic Silicate Covalent Organic Framework with srs Topology. *J. Am. Chem. Soc.* **2018**, *140* (16), 5330−5333.
(29) Fang, Q.; Gu, S.; Zheng, J.; Zhuang, Z.; Qiu, S.; Yan, Y. 3D Microporous Base-Functionalized Covalent Organic Frameworks for Size-Selective Catalysis. *Angew. Chem., Int. Ed.* **2014**, *53* (11), 2878−2882.
(30) Wang, H.; Zeng, Z.; Xu, P.; Li, L.; Zeng, G.; Xiao, R.; Tang, Z.; Huang, D.; Tang, L.; Lai, C.; Jiang, D.; Liu, Y.; Yi, H.; Qin, L.; Ye, S.; Ren, X.; Tang, W. Recent progress in covalent organic framework thin films: fabrications, applications and perspectives. *Chem. Soc. Rev.* **2019**, *48* (2), 488−516.
(31) Lohse, M. S.; Bein, T. Covalent Organic Frameworks: Structures, Synthesis, and Applications. *Adv. Funct. Mater.* **2018**, *28* (33), 1705553.
(32) Ma, X.; Scott, T. F. Approaches and challenges in the synthesis of three-dimensional covalent-organic frameworks. *Commun. Chem.* **2018**, *1* (1), 98.
(33) Diercks, C. S.; Yaghi, O. M. The atom, the molecule, and the covalent organic framework. *Science* **2017**, *355* (6328), eaal1585.
(34) Fan, H.; Gu, J.; Meng, H.; Knebel, A.; Caro, J. High-Flux Membranes Based on the Covalent Organic Framework COF-LZU1 for Selective Dye Separation by Nanofiltration. *Angew. Chem., Int. Ed.* **2018**, *57* (15), 4083−4087.
(35) Fan, H.; Mundstock, A.; Feldhoff, A.; Knebel, A.; Gu, J.; Meng, H.; Caro, J. Covalent Organic Framework−Covalent Organic Framework Bilayer Membranes for Highly Selective Gas Separation. *J. Am. Chem. Soc.* **2018**, *140* (32), 10094−10098.
(36) Li, G.; Zhang, K.; Tsuru, T. Two-Dimensional Covalent Organic Framework (COF) Membranes Fabricated via the Assembly of Exfoliated COF Nanosheets. *ACS Appl. Mater. Interfaces* **2017**, *9* (10), 8433−8436.
(37) Dey, K.; Pal, M.; Rout, K. C.; Kunjattu H, S.; Das, A.; Mukherjee, R.; Kharul, U. K.; Banerjee, R. Selective Molecular Separation by Interfacially Crystallized Covalent Organic Framework Thin Films. *J. Am. Chem. Soc.* **2017**, *139* (37), 13083−13091.
(38) Kim, S.; Lim, H.; Lee, J.; Choi, H. C. Synthesis of a Scalable Two-Dimensional Covalent Organic Framework by the Photon-Assisted Imine Condensation Reaction on the Water Surface. *Langmuir* **2018**, *34* (30), 8731−8738.
(39) Bisbey, R. P.; DeBlase, C. R.; Smith, B. J.; Dichtel, W. R. Two-dimensional Covalent Organic Framework Thin Films Grown in Flow. *J. Am. Chem. Soc.* **2016**, *138* (36), 11433−11436.
(40) Rotter, J. M.; Weinberger, S.; Kampmann, J.; Sick, T.; Shalom, M.; Bein, T.; Medina, D. D. Covalent Organic Framework Films through Electrophoretic Deposition-Creating Efficient Morphologies for Catalysis. *Chem. Mater.* **2019**, *31*, 10008−10016.
(41) Becker, D.; Heidary, N.; Horch, M.; Gernert, U.; Zebger, I.; Schmidt, J.; Fischer, A.; Thomas, A. Microporous polymer network films covalently bound to gold electrodes. *Chem. Commun.* **2015**, *51* (20), 4283−4286.
(42) Ma, T.; Kapustin, E. A.; Yin, S. X.; Liang, L.; Zhou, Z.; Niu, J.; Li, L.-H.; Wang, Y.; Su, J.; Li, J.; Wang, X.; Wang, W. D.; Wang, W.; Sun, J.; Yaghi, O. M. Single-crystal x-ray diffraction structures of covalent organic frameworks. *Science* **2018**, *361* (6397), 48−52.
(43) Evans, A. M.; Parent, L. R.; Flanders, N. C.; Bisbey, R. P.; Vitaku, E.; Kirschner, M. S.; Schaller, R. D.; Chen, L. X.; Gianneschi, N. C.; Dichtel, W. R. Seeded growth of single-crystal two-dimensional covalent organic frameworks. *Science* **2018**, *361* (6397), 52−57.
(44) Lee, S.; Uliana, A.; Taylor, M. K.; Chakarawet, K.; Bandaru, S. R. S.; Gul, S.; Xu, J.; Ackerman, C. M.; Chatterjee, R.; Furukawa, H.; Reimer, J. A.; Yano, J.; Gadgil, A.; Long, G. J.; Grandjean, F.; Long, J. R.; Chang, C. J. Iron detection and remediation with a functionalized porous polymer applied to environmental water samples. *Chem. Sci.* **2019**, *10* (27), 6651−6660.
(45) Lu, W.; Yuan, D.; Sculley, J.; Zhao, D.; Krishna, R.; Zhou, H.-C. Sulfonate-Grafted Porous Polymer Networks for Preferential CO2 Adsorption at Low Pressure. *J. Am. Chem. Soc.* **2011**, *133* (45), 18126−18129.
(46) Schmidt, J.; Werner, M.; Thomas, A. Conjugated Microporous Polymer Networks via Yamamoto Polymerization. *Macromolecules* **2009**, *42* (13), 4426−4429.
(47) Welty, J. R.; Wicks, C. E.; Wilson, R. E.; Rorrer, G. L. *Fundamentals of Momentum, Heat, and Mass Transfer*, 4th ed.; John Wiley & Sons, Inc.: New York, 2001.
(48) Thomas, J. M. H.; Trewin, A. Amorphous PAF-1: Guiding the Rational Design of Ultraporous Materials. *J. Phys. Chem. C* **2014**, *118* (34), 19712−19722.
(49) Shi, Q.; Sun, H.; Yang, R.; Zhu, Z.; Liang, W.; Tan, D.; Yang, B.; Li, A.; Deng, W. Synthesis of conjugated microporous polymers for gas storage and selective adsorption. *J. Mater. Sci.* **2015**, *50* (19), 6388−6394.

https://dx.doi.org/10.1021/jacs.9b10884
J. Am. Chem. Soc. 2020, 142, 6548−6553